Systematic study of high-order harmonic optimal control by temporal pulse shaping of laser pulses

O. Boyko,[1,2] C. Valentin,[1] B. Mercier,[1] Ch. Coquelet,[1] V. Pascal,[1] E. Papalazarou,[1] G. Rey,[1] and Ph. Balcou[1,3]
[1]*Laboratoire d'Optique Applique, ENSTA, Ecole Polytechnique, CNRS, F-91761 Palaiseau, France*
[2]*Laboratoire de Photonique et Nanostructures, CNRS UPR20, Route de Nozay, 91460 Marcoussis, France*
[3]*Centre Lasers Intenses et Applications, Universit de Bordeaux 1, CNRS, CEA, 351 Cours de la libration, F-33405 Talence, France*
(Received 18 July 2007; published 14 December 2007)

We explore experimentally and numerically the physics underlying the optimization of high-order harmonic generation by intense laser pulses, whose temporal profile is tailored by a learning genetic algorithm. Based on a large set of optimization data obtained under different generation parameters, we show that the algorithm converges toward a class of very special profiles on the leading edge of the pulse. The behavior of the harmonic signal is then compared with theoretical simulations based on the time-dependent Schrödinger equation, allowing one to identify separately the role of microscopic and macroscopic phenomena in the temporal dynamics of high-harmonic generation and optimization.

DOI: 10.1103/PhysRevA.76.063811 PACS number(s): 42.65.Ky, 42.65.Re

I. INTRODUCTION

High-order harmonics generation (HHG) is a highly nonlinear process occurring when an intense linearly polarized laser field interacts with an atomic gas. High-order harmonic generation has become a standard technique for producing extreme ultraviolet radiation in the 5–50 nm wavelength, thus opening the field of attosecond atomic, molecular and optical physics. Much of the basic physics is now well understood, in spite of the intricacy of the process, which involves both subtle quantum effects at the single atom level, and complex phase matching issues between the driving laser field and the harmonics [1]. Two main trends may be distinguished in the current research in this field. The first is the general push toward the generation and control over single attosecond pulses, largely thanks to progress in laser technology, that provides methods to amplify laser pulses as short as two optical cycles, and to play with the polarization vector of the light to prevent attosecond pulses generation except in a controlled temporal gate [2,3]. The second trend is to further increase the yields of extreme UV radiation, as required to ease the ongoing applications of this femtosecond or attosecond source to other scientific domains. The aim is to produce high-order harmonic sources beyond the micro-Joule level [4,5], with very good spatial and temporal coherence, and short pulse duration. In order to increase the yield to such levels, high-order harmonics may be generated with an intense laser system delivering 25–100 fs pulses, and having up to 100 mJ of energy per pulse. Such high energies allow for a very loose focusing of the beam [5,7], resulting in an extremely homogeneous phase matching along the interaction region, very much like guided propagation in hollow-core fibers [6,8]. However, it was also considered whether one could enhance the yield of the process by an active control of the laser parameters. This refers not only to harmonic signal optimization through a detailed analysis of the generation characteristics, such as propagation geometry, gas species, and density or/and medium geometry; but also to much more complex methods to control the laser pulses through temporal or spatial shaping of laser pulses. Harmonic signal optimal control by temporal pulse shaping was first proposed by Bartels *et al.* [9], followed by Reitze *et al.*[10]. More recently, "closed-loop" optimal control experiments have shown that specific orders near cutoff can be enhanced through temporal laser shaping [11]. Closed-loop optimal control is based on the use of evolutionary algorithm that searches spectral phase configurations to produce the desired harmonic output. This method permits us to easily find the best solution of a complex multiparameter problem which is not evident a priori, and does not require any knowledge of the system. Closed-loop optimal control was therefore used to increase a brightness of one given harmonic order, and was demonstrated to be very efficient to gain a factor of 10 on signal maximum. We concentrate on a different goal, namely, the optimization of absolute photon number, irrespective for the phase of the harmonic radiation, as this is one of the most important parameters for most applications of high-order harmonics radiation. As often emphasized, the physics underlying the optimization process may be of considerable interest, provided one may find methods to unravel it from the optimization data. Bartels *et al.* [12] have underlined phase effects, of direct impact on the temporal phase of high-order harmonics emitted by single atoms, and henceforth on the spectral brightness of the measured harmonic peaks. We present here the first systematic study of the complex influence of temporal shaping of a laser pulse on the total high-order harmonic generation yield, including both the single atom response and phase matching. This is achieved by interplay between experimental optimization data obtained in a wide range of generation parameters, and numerical simulations describing the atomic response and phase matching, using as an input the experimentally obtained optimal laser temporal profiles. This allows us both to control harmonic photon number via laser temporal shaping, and to unravel the microscopic and macroscopic mechanisms driving the optimization. The paper is organized as follows. In Sec. II, we describe the laser system, the experimental apparatus, and procedure. The main experimental results, consisting of systematic studies of harmonic signal evolution with temporal shaping of laser pulse are presented in Sec. III

and discussed in Sec. IV on the basis of comparisons with numerical simulations. We summarize and conclude in Sec. V.

II. DESCRIPTION OF THE EXPERIMENT

The laser used is a 1 kHz repetition rate Ti-sapphire system, based on chirped pulse amplification producing 6 mJ, 40 fs pulses, at 810 nm. An acousto-optical programmable filter (Dazzler^{TM}) located before the first amplifier stage is placed to control the pulse spectral phase and, thus, a temporal profile of laser pulse. In principle, such a filter can be used to modify also the spectrum (spectral amplitude) of the laser pulse: The shaping of the laser spectrum is reached by varying of the acoustical wave power in the filter crystal and usually used to compensate the gain narrowing effect during laser amplification [13]. In this experiment we perform the temporal shaping only with spectral phase because the phase is less influenced by further amplification in crystals than spectral amplitude. The spectral phases of the pulses at the output of the laser system are measured by the SPIDER method [14]. We checked that spectral phases imposed by the Dazzler^{TM} correspond exactly to those measured by the SPIDER, demonstrating a reliable calibration of the SPIDER and a low level of nonlinear B integral in our laser system [14,15]. The learning algorithm optimizes the output HHG flux by searching the best spectral phase. The spectral phase is parametrized by ten arbitrary values across the spectrum (bounded in the range of 0 to 2π) and two value ϕ_2 and ϕ_3, the second- and third-order Taylor coefficients. This parametrization is chosen to provide a sufficiently complex phase structure while working within the limitations of the acousto-optical programmable filter. A fitness function is defined, based on a fit of each individual harmonic peak as a Gaussian function specified by its wavelength, height, and width, with appropriate weight and sensitivity to fit. The value of this function allows one to compare the experimental spectrum with a desired one and to observe convergence or nonconvergence of the learning algorithm. From the fit parameters, a large number of fitness functions may be chosen, in order to optimize the peak brightness, or the rejection of neighboring harmonics, or the central harmonic wavelength, etc. We concentrate on a fitness function basically related to the area of the harmonic profile in a given spectral window, which yields the best possible estimate of the total photon flux for that particular harmonic. It is important to note that before starting any optimal control we correct the intrinsic laser phase, by imposing the reverse of the uncorrected laser spectral phase. The starting point of all optimizations is hence a Fourier transform-limited pulse with a quasiflat spectral phase to within 0.25 rad.

After passing through a variable-diameter aperture, the beam is focused by a 1 m focal length lens into the vacuum system containing a 2 mm length gas cell (Fig. 1). The IR beam and the harmonics generated in the gas cell copropagate towards a XUV spectrometer. The IR beam is blocked between the gas cell and the spectrometer using two 300-nm-thick aluminium filters. The XUV spectrometer is composed of a 1 m focal length gold coated toroidal mirror and an

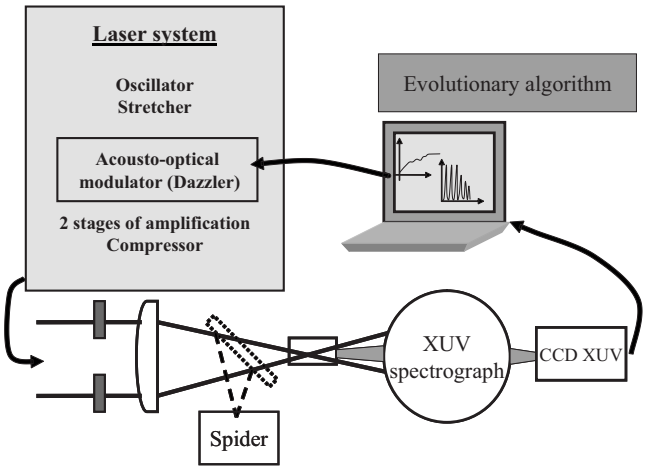

FIG. 1. Experimental setup.

XUV grating at grazing incidence. The signal is measured by a back illuminated XUV CCD device, enabling an absolute calibration [16], only limited by the unknown aging of the CCD sensor, which can only lead to an underestimation of the flux. The experiment proceeds in three steps. Before using the optimization algorithm, we first optimize at best the harmonic signal by adjusting macroscopic generation parameters such as gas pressure, lens position, and iris diameter. The resulting number of photons is as high as 10^8 photons per shot for H25 at the source. The effects of these parameters on HHG are multiple, coupled, and not trivial. For instance, the variation of iris aperture results in a geometrical increase of focal zone and consequently in a larger volume of laser-gas interaction. Kazamias *et al.* [16] have demonstrated that a small iris aperture configuration gives rise to very similar conditions of generation than a capillary [6], in the sense that phase matching is kept homogenous over the whole interaction zone. The gas density is the other important parameter for harmonic generation: From a microscopic point of view, higher density corresponds to higher number of emitting atoms, while from a macroscopic point of view, higher density induces an increase of the absorption of the generated XUV light and affects phase matching via the atomic and electronic dispersion terms. The third parameter—focal point position with respect to the cell entrance—plays an important role in optimization as well. This parameter leads not only to a variation of the intensity level in the interaction zone, but also to changes in the laser wave vector and the gradient of intensity, which affects phase matching. In a second step, we explore harmonic optimal control via laser pulse shaping in these macroscopic optimal conditions. We record the evolution of the fitness function along with the generation number in the genetic algorithm, as well the optimal high-order harmonic spectra, and the laser spectral phase in the final conditions. In the final step, we perform a series of experiments for slightlydifferent values of iris diameter, gas pressure and position of focusing lens, in order to go further in understanding the major mechanisms of photon yield enhancement, and in studying the influence of these three parameters on adaptive control optimization. This crucial last step, which is essen-

tially the only one detailed below, is meant to allow us to disentangle the roles of microscopic processes and of phase-matching effects on the harmonic optimization.

III. EXPERIMENTAL RESULTS

Two spectral ranges, interesting from an application point of view, were explored in this study. The first range is around 32 nm corresponding to the 25th harmonic generated in argon, for which the conversion efficiency is highest (about 10^{-5} [8]). The second spectral range corresponds to the highest orders (around the 41st harmonic) that pass through aluminium filter and are observed in the experiment. For H25 generated in the cell at a pressure of 22 mbar of argon, the signal maximum is obtained for an iris diameter of 16 mm (laser energy=1.8 mJ, Rayleigh length=10 mm), and for a cell placed 2 mm after the laser focus, resulting in a peak intensity in the cell of 10^{14} W/cm^2, much lower than the ionization saturation intensity for Ar. In all conditions for the study of the 41st harmonic, and in the conditions just mentioned for the 25th, the learning algorithm resulted in a significant but moderate enhancement of the integrated harmonic flux. The ratio between the integrated fluxes before and after laser optimization (gain factor) is generally about 2 for the 41st harmonic, and for the 25th harmonic in those low intensity conditions. The algorithm is then always observed to converge towards a near Fourier-limited pulse, for which intensity in the medium is maximal, with better accuracy than the SPIDER based suppression of the laser spectral phase. Note, however, that the gain factor can reach values as high as 10 if the initial temporal shape is not Fourier-limited, that is, if the procedure consisting of bringing the spectral phase to zero based on a SPIDER measurement is not followed, even though the pulse duration as measured by the SPIDER may seem hardly larger than its Fourier-limited value, namely, typically 45 fs instead of 40 fs.We will concentrate in the following on the photon yield optimization of harmonic 25, because it leads to the most interesting results about high-order harmonic generation physics. We have preformed three systematic studies of H25 signal optimization versus (i) iris diameter, (ii) gas pressure, and (iii) focus-cell distance.

In order to study the gain factor variations versus the iris diameter, other series of optimal control were performed with iris apertures of 18.5 and 20 mm. For all these experiments, the peak intensity in the cell is estimated to 1.5×10^{14} W/cm^2 and 1.8×10^{14} W/cm^2, respectively, which is still under the intensity of barrier suppression for the first ionization level of Ar, $I_{\mathrm{BSI}}=2.3\times10^{14}$ W/cm^2. Figures 2(a)–2(c) shows the evolution of harmonic spectra for three harmonics (23rd–27th) during 14 iterations. The most efficient optimization was observed for an iris aperture of 18.5 mm, yielding a gain factor of 3 for the integrated flux, whereas this factor is 2 for the 20 mm aperture. The convergence time of the algorithm is about 15 to 20 minutes.

Figures 2(d)–2(f) presents the evolution of the integrated H23–H27 signal over the generations. Finally, the comparison between the best 25th harmonic integrated signal before learning algorithm optimization (iris diameter=16 mm, pressure=22 mbar, focus position=2 mm) and the best signal after optimization (iris diameter=18.5 mm, pressure =22 mbar, focus position=2 mm) is about 2.5.

The measurements of temporal profiles of the IR pulse corresponding to the final results of the three optimal control series are illustrated on Fig. 3. The initial pulse is represented by a solid line and corresponds to the starting point of algorithm. A negative time corresponds to the beginning of pulse. Figure 3 emphasizes one surprising tendency, general for all three optimizations: The algorithm performs a complex spectral phase manipulation to get a pulse temporal profile with a quasilinear leading edge slope. Thus an increase of the iris diameter is accompanied by the optimized pulse becoming longer and the leading edge is getting gently sloping.

Another set of experiments was performed to study the signal of H25 before and after optimizations versus gas pressure (Fig. 4). The argon pressure inside the generating cell is varying from 10 to 30 mbar. At even larger values of gas pressure, the processes of XUV reabsorption and ionization-induced defocusing start to play an important role, limiting the yield to the so-called absorption limit, and making the propagation too complex for the present study. For an aperture diameter fixed to 18.5 mm, the gain factor is about 2 for high pressures and equal to 1.7 for 10 mbar and 15 mbar: Figure 4(a) shows a linear interpolation of gain factor over pressure values. There is clearly no essential difference between high- and low-pressure conditions for gain factor and, interestingly, the final pulses for 10 mbar optimization and for 30 mbar optimization are measured to have the same temporal shape [Fig. 4(b)]. This leads us to the first main conclusion that phase-matching effects related to atomic or electronic densities do not play a major role in the optimization process. However, it is not possible to conclude at this stage that phase matching is passive in the optimal control, as will be clear from the following.

Finally, we have performed a study of the optimization process versus cell entrance with respect to the laser focus. Figure 5 presents the harmonic yield for different focal point positions, before and after the optimal control process, and the ratio between them. Here, the iris diameter is 18 mm, corresponding to a Rayleigh range of 8.8 mm, and the gas pressure is 22 mbar. Before the laser shape optimization we observe a maximum of signal when the laser is focused at the cell entrance. When the cell is placed 8 mm after the focus, the intensity is nearly divided by 2, so that H25 reaches the cutoff regime and the signal drops. After the optimal control, we note that the signal is maximal when the cell is placed 6 mm after the focus. Moreover, the signal ratio after and before the learning algorithm optimization increases when the cell is placed far away from the focus, where the intensity is low and the intensity longitudinal gradient is high. We deduce that the optimal control process does depend on phase-matching, through a process that has to be related to the intensity gradient. The experimental data above show that as the learning algorithm finds pulses that enhance the 25th harmonic, the yields of the 23rd and 27th harmonic orders increase accordingly. The algorithm is very effective at increasing the brightness of the 25th–27th harmonics by nearly an order of magnitude and the integrated photon number by factor 2 to 6 (Fig. 5), by means of a combination of

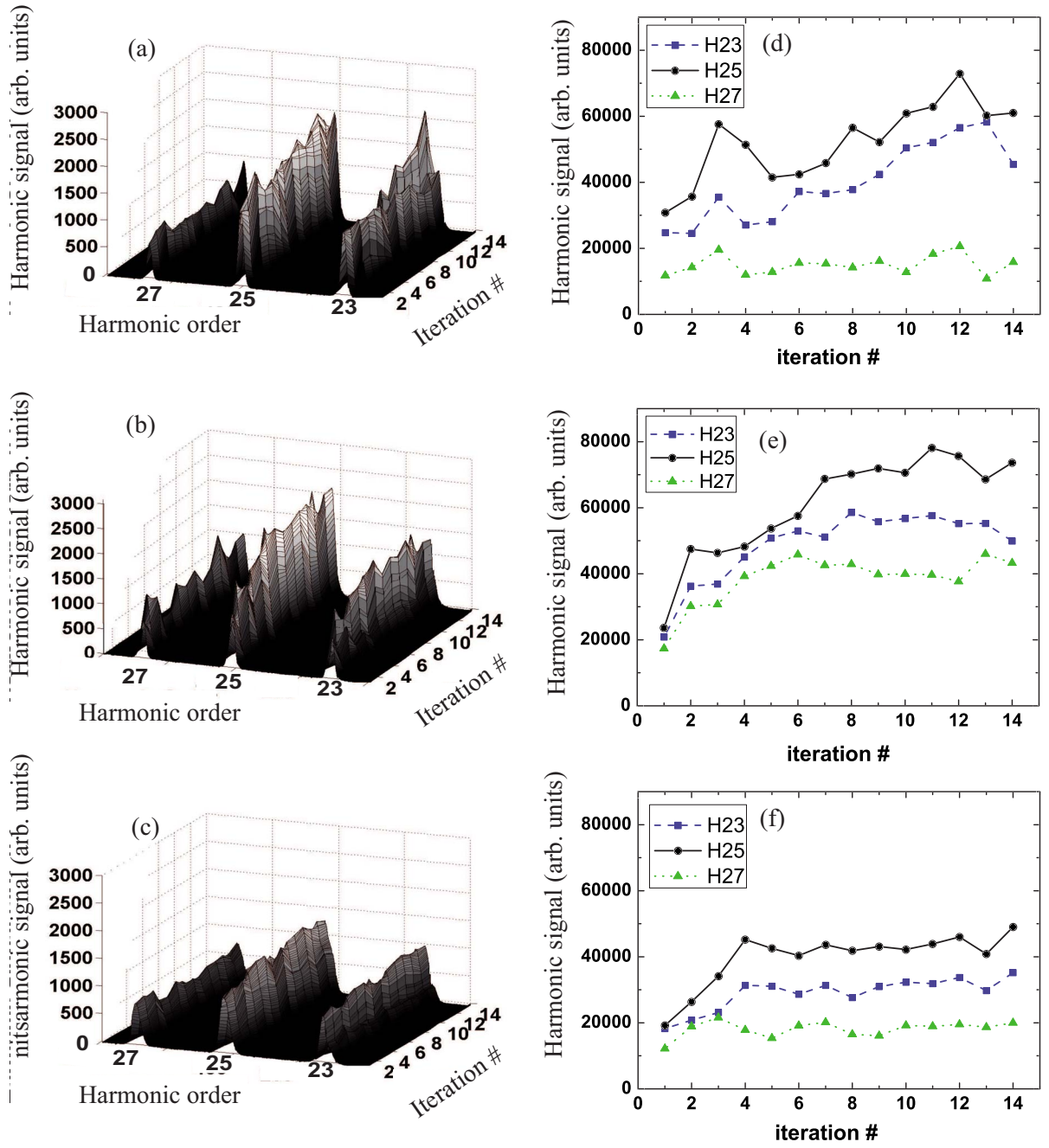

FIG. 2. (Color online) H23-H27 spectra evolution during optimal control for iris apertures (a) 16 mm, (b) 18.5 mm, and (c) 20 mm. Evolution of integrated harmonics signal for iris aperture of 16 mm (d), 18.5 mm (e), and 20 mm (f).

microscopic and macroscopic processes. Our experimental results show that the complex spectral phase optimizations result in a family of quite particular temporal shapes of laser pulse, exhibiting a quasilinear leading edge slope, with a smaller time derivative as for a Gaussian pulse. Thus our experimental data confirm that the Gaussian profile of laser pulses is not optimal for efficient high-order harmonic generation for this spectral range, unless the initial laser intensity is fairly low.

IV. DISCUSSION

In order to understand the physics underlying the optimization in the various conditions explored experimentally, we resort to numerical simulations of the HHG process, both at the single atom level, and at the macroscopic propagation and phase-matching level.

We first compute the atomic response of the noble gas to the shaped laser pulses. The atomic dipole acceleration is calculated by solving the time-dependent Schrödinger equation (TDSE) for one active electron along one dimension. The principle of TDSE code has been first proposed by Kulander *et al.* [17]; we use an implementation developed by Véniard and Taieb [18]. The dipole acceleration for a single argon atom is calculated in the case of interaction with an IR laser pulse, in the velocity gauge. The program is based on time propagation of the spatial wave function for one active

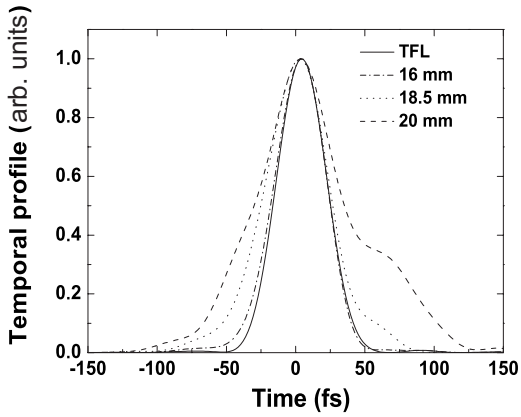

FIG. 3. Temporal laser shape after each optimal control for different iris diameter. Solid line: Fourier-limited pulse; dash-dotted line: 16 mm iris diameter; dotted line: 18.5 mm iris diameter; dashed line: 20 mm iris diameter.

electron in a 1D colombian potential. The wave function is discretized in space and time. Then we calculate the mean value of the dipole acceleration for this wave function. As we will see, 1D calculations have been sufficient to explain our experimental results. So, 3D calculations have not been developed for this purpose. Experimentally, the learning algorithm reshapes the driving laser pulse to optimize the fitness function; as we have measured the spectrum and the spectral phase of all reshaped laser pulses, we can easily introduce them into the TDSE simulations. Figure 6 shows the calculated dipole emission versus time for each optimized pulse shape given by the experiment with varying aperture, corresponding to Fig. 2. As one can see, the harmonics are generated principally at the leading edge of the pulse, where the instantaneous intensity is not large enough to ionize the medium. At the top of the pulse, high ionization levels deplete the neutral medium and spoil the generation. It is important to realize that the dipole emission is longer in the case of the optimized pulse than for the nonoptimized one and that the algorithm adjusts the laser pulse to ensure almost the same amplitude of dipole emission.

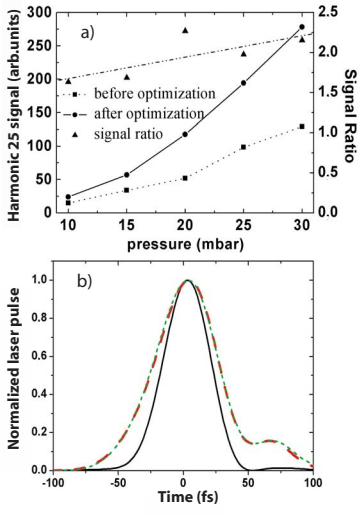

FIG. 4. (Color online) (a) Harmonic integrated signals before and after laser optimal control vs gas pressure P (dots and square: nonoptimized signal; solid line and circles: optimized signal; triangles: ratio between optimized and nonoptimized signals; solid slope: guide to the eyes for signal ratio). (b) Laser intensity profile before (solid line) and after optimal control (dotted line corresponds to optimal control for $P=15$ mbar; dashed line corresponds to optimal control for $P=30$ mbar).

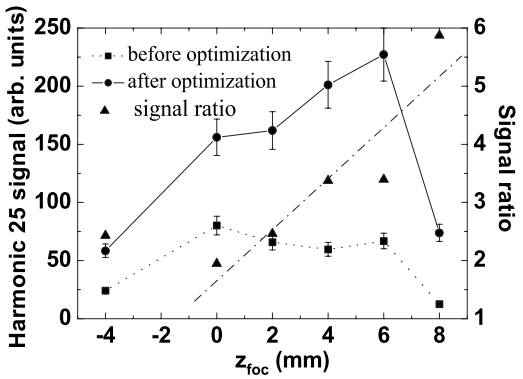

FIG. 5. Optimal signals vs cell entrance with respect to laser focus (dots and square: nonoptimized signal; solid line and circles: optimized signal; triangles: ratio between optimized and nonoptimized signals; solid slope: guide to the eyes for signal ratio).

When the iris diameter increases, the leading edge slope decreases and the laser pulse duration increases: The total intensity remains constant when the transmitted energy increases. The ionization probability is maintained at a low value and remains weak for a longer time at the pulse leading edge. Consequently, the harmonic signal is generated during more optical cycles than for the nonoptimized case. However, by finding a smooth leading edge of pulse using the learning algorithm, one obtains a relatively long harmonic emission: Figure 7 shows the theoretical values of XUV emission duration calculated before and after the optimal control experiment for different apertures. These data demonstrate that the enhancement of harmonic photon yield is involved by increasing the optical cycle number participating in harmonic generation. Thus a theoretical analysis of the data can validate the mechanism for learning algorithm optimization. Even though this behavior was not known or predicted previously but was rather discovered by the experimental optimization process, we note this ability to enhance HHG using shaped light pulses is quite consistent and natural with our understanding of the physics of HHG. During the leading edge of a transform-limited laser pulse, the increasing laser intensity leads to a rapidly increasing gas ionization and, generally, at the peak of the pulse there are no neutral atoms enough to generate harmonics. The rapid ionization is partially delayed by adjusting the temporal intensity profile of the laser during optimization processes. Thus the harmonic generation occurs during a larger number of laser optical cycles and a significant enhancement of the harmonic yield is observed.

After this first explanation in terms of single atom response, we focus on the macroscopic effects and especially on phase matching. We have performed a one-dimensional calculation of the time varying mismatch between the phase

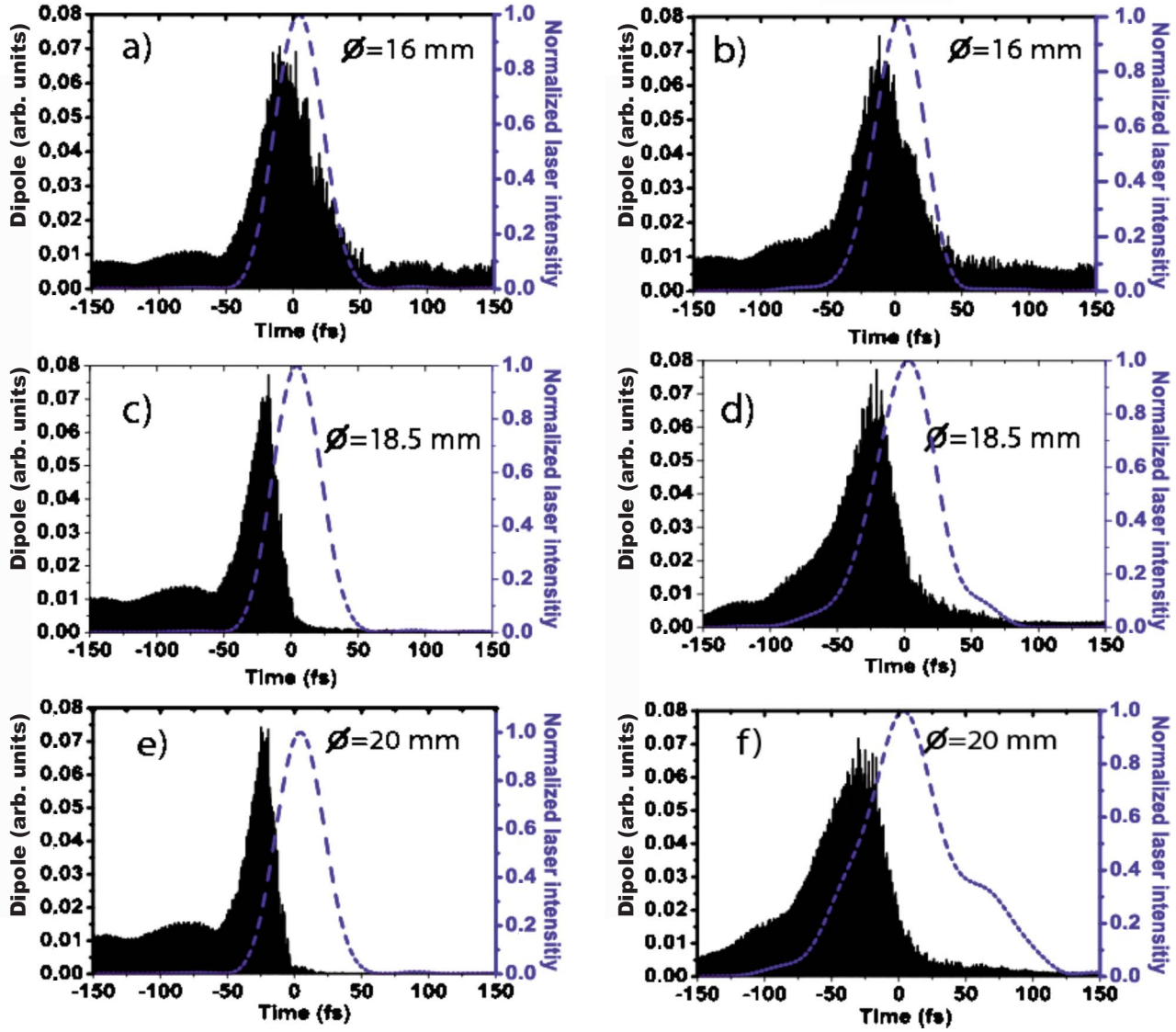

FIG. 6. (Color online) HHG emission in time for (a), (c), (e) initial and (b), (d), (f) optimally-stopped laser pulses for different iris diameters.

of the harmonic radiation of 25th harmonic and the infrared laser phase. Phase-matching of a harmonic q occurs when the qth harmonic wave vector k_q and the induced polarization in the medium due to the laser field are equal. We define the mismatch δk which is the result of the contributions of the Gouy phase induced by focusing the infrared beam, the atomic and electronic dispersions, and the atomic phase (intrinsic phase of the harmonic radiation) [19]. The result can be expressed in terms of propagation wave vectors as follows [20]:

$$\delta k = \nabla \phi_q = k_q - q k_{\text{laser}} + \delta \phi_{\text{at}}, \tag{1}$$

where q is the harmonic order and k_q and k_{laser} are harmonic and laser wave vectors. From the plasma dispersion formula, we have

$$n_{\text{laser}} = 1 - \frac{n_e}{2 n_c \omega_{\text{laser}}}, \tag{2}$$

where n_e is the ionization probability and n_c is the critical plasma density at a given wavelength. We neglect the plasma dispersion at the harmonic wavelength ($k_q = q\omega/c$). The influence of focusing the laser on k_{laser} is taken into account by the Gouy phase gradient. Accordingly, the time varying wave vector mismatch is given by

$$\delta k = q \frac{\omega}{c} \left(\frac{n_e}{2 n_c} - \delta n_{\text{at}} \right) - q \phi_{\text{Gouy}} + \delta \phi_{\text{at}}. \tag{3}$$

The first term of this equation corresponds to the electronic and atomic dispersions, the electronic density is calculated by instantaneous ADK ionization rates [21]; the second one is the geometric term (gradient of the Gouy phase). The third term is substantial to understand phase matching in

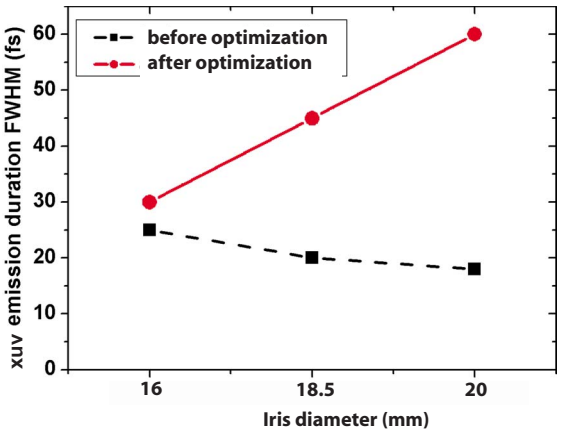

FIG. 7. (Color online) XUV emission FWHM duration calculated for optimized laser pulse (circles) and initial gauss pulse (squares) for three aperture diameters: 16 mm, 18.5 mm, and 20 mm.

our experimental configuration: It proportional to intensity gradient [19] and changes sign when the cell is placed before and after the laser focus. We define the coherence length as the length over which the dipoles emission generated at different points in the gas medium destructively interferes. It is given by

$$L_{\mathrm{coh}} = \frac{\pi}{\delta k}. \tag{4}$$

This definition of coherence allows to find phase-matching conditions and also to calculate their time-dependent evolution. Turning back to experimental data, we have calculated the coherence length versus time for 18.5 mm iris diameter and for the experiment with varying gas pressure and lens position. Phase matching occurs when the coherence length is greater than the cell length (in our

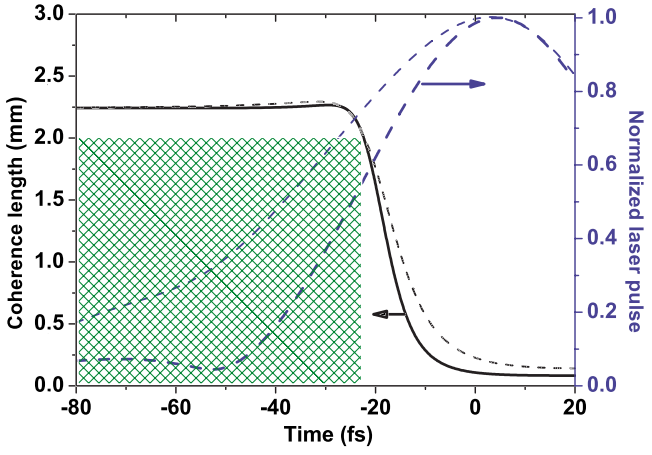

FIG. 8. (Color online) Coherence length evolution for H25 generated in argon (iris 18.5 mm) before optimal control (solid line) and after optimal control (thin dashed line); measured pulse envelope before optimization (thick dashed line) and after optimization (thin dashed line); the hatched zone corresponds to good phase matching.

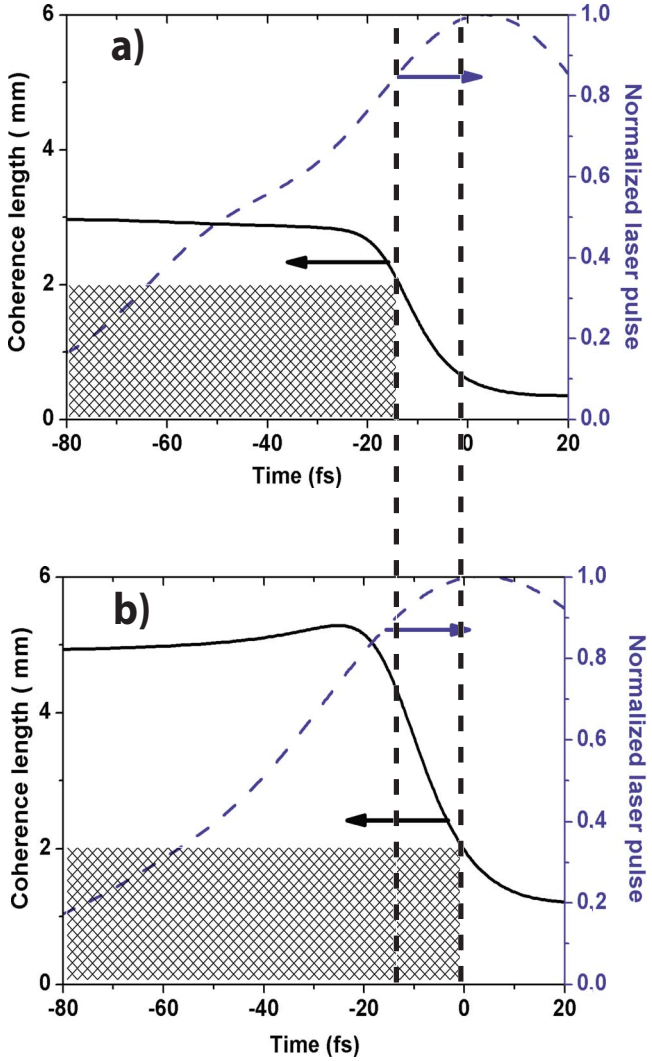

FIG. 9. (Color online) Optimized case: Coherence length evolution for H25 generated in argon for (a) $z_{\mathrm{foc}}=6$ mm and (b) $z_{\mathrm{foc}}=-4$ mm. The dotted line corresponds to the measured pulse envelope and the hatched zone corresponds to good phase matching.

experimental conditions $L_{\mathrm{cell}}=2$ mm). Figure 8 shows the temporal evolution of the coherence length for optimized-nonoptimized laser pulses corresponding to a 18.5 mm aperture condition.

In both cases of Fig. 8, the time span of phase matching is similar: Phase matching lasts until near −22 fs with respect to the peak of the pulse. Thus this comparison leads to the conclusion that the optimization involves only microscopic processes described above. We confirm by calculating the coherence length for different pressures (10 mbars and 30 mbars) that phase matching does not play a role for optimization. The duration of good phase-matching is rather the same for the two pressure values. In this case, the signal increase is only due to the microscopic response.

We now simulate the experimental data from the variation in focusing lens position (Fig. 5). We consider only two cases: $z_{\mathrm{foc}}=-4$ mm and $z_{\mathrm{foc}}=6$ mm. The time span for good phase matching is shown on Fig. 9 and corresponds to $L_{\mathrm{coh}} > L_{\mathrm{cell}}$ (2 mm). Indeed, better phase matching occurs for

a time interval much longer for $z_{foc}=6$ mm than for $z_{foc}=-4$ mm. Only for a cell placed after the focus, the dipole phase gradient counterbalances the electronic dispersion and L_{coh} is higher. Comparing the duration for good phase matching for the two positions of the cell, one notes that for $z_{foc}=6$ mm it lasts 15 fs longer than for $z_{foc}=-4$ mm. The phase-matching temporal gate is also enhanced and the algorithm allows building constructively the harmonic signal for a longer time. Combining both effects, we have explained that the optimization process rests on longer dipole emission and longer phase matching.

V. CONCLUSION

In conclusion, we have explored experimentally and numerically how the active control of the laser spectral phase may enhance the high-order harmonic flux. Starting from laser pulses close to the Fourier limit, we have shown that the optimization procedure has completely different effects when the laser intensity is rather low, or when it is sufficiently high that the laser temporal shape may be modified while keeping the intensity in the correct range for high-order harmonics. In the former case, the algorithm converges towards the real Fourier-limited pulses, as experienced by the nonlinear medium. In the latter case, the optimization results in a tailored temporal laser profile, with a leading edge shaped into a gentle slope that allows for a much longer duration for effective high-order harmonic generation, thus resulting in an increase of the XUV photon number by a factor up to 6, and more often between 2 and 3. Analysis of the complete data sets were used to study the role of microscopic and macroscopic parameters of generation dynamics and to validate this mechanism. In particular, the systematic study versus the cell entrance position with respect to the laser focus has shown that phase-matching effects play an indirect but essential role in the pulse optimization: In the conditions where the phase matching lasts longer, the algorithm converges to better optimization solution. Thus phase matching acts as a temporal gate which permits the learning algorithm to shape a laser pulse profile inside its limits.

How to recover the physics underlying an optimization based on a learning algorithm is a very difficult question. Our proposal, based on an interplay between experimental optimal control data and numerical simulations, has allowed us to unravel the role of phase matching defining a temporal gate; this is very complementary to other approaches, based on the statistical analysis of the optimization data. All those approaches should help enormously to control and increase further the yields of high harmonics, now considered as an efficient source of femtosecond or attosecond radiation, to be applied to many scientific fields.

ACKNOWLEDGMENTS

The authors thank Marie Curie Research Training Networks XTRA (MRTN-CT-2003-505138) for financial support.

[1] T. Brabec and F. Krausz, Rev. Mod. Phys. **72**, 545 (2000).
[2] I. J. Sola, E. Mvel, E. Elouga, E. Constant, V. Strelkov, L. Poletto, P. Villoresi, E. Benedetti, J.-P. Caumes, S. Stagira, C. Vozzi, G. Sansone, and M. Nisoli, Nat. Phys. **2**, 319 (2006).
[3] G. Sansone, E. Benedetti, F. Calegari, C. Vozzi, L. Avaldi, R. Flammini, L. Poletto, P. Villoresi, C. Altucci, R. Velotta, S. Stagira, S. De Silvestri, and M. Nisoli, Science **314**, 443 (2006).
[4] J.-F. Hergott, M. Kovacev, H. Merdji, C. Hubert, Y. Mairesse, E. Jean, P. Breger, P. Agostini, B. Carre, and P. Salieres, Phys. Rev. A **66**, 021801(R) (2002).
[5] H. T. Kim, I. J. Kim, V. Tosa, Y. S. Lee, and C. H. Nam, Appl. Phys. B: Lasers Opt. **78**, 863 (2004).
[6] C. G. Durfee III, A. R. Rundquist, S. Backus, C. Herne, M. M. Murnane, and H. C. Kapteyn, Phys. Rev. Lett. **83**, 2187 (1999).
[7] E. Takahashi, Y. Nabekawa, T. Otsuka, M. Obara, and K. Midorikawa, Phys. Rev. A **66**, 021802(R) (2002).
[8] S. Kazamias, D. Douillet, F. Weihe, C. Valentin, A. Rousse, S. Sebban, G. Grillon, F. Aug, D. Hulin, and Ph. Balcou, Phys. Rev. Lett. **90**, 193901 (2003).
[9] R. Bartels, S. Backus, E. Zeek, L. Misoguti, G. Vdovin, I. P. Christov, M. M. Murnane, and H. C. Kapteyn, Nature (London) **406**, 164 (2000).
[10] D. H. Reitze, S. Kazamias, F. Weihe, G. Mullot, D. Douillet, F. Aug, O. Albert, V. Ramanathan, J.- P. Chambaret, D. Hulin, and P. Balcou, Opt. Lett. **29**, 86 (2004).
[11] P. Villoresi, S. Bonora, M. Pascolini, L. Poletto, G. Tondello, C. Vozzi, M. Nisoli, G. Sansone, S. Stagira, and S. De Silvestri, Opt. Lett. **29**, 207 (2004).
[12] R. A. Bartels, M. M. Murnane, H. C. Kapteyn, I. Christov, and H. Rabitz, Phys. Rev. A **70**, 043404 (2004).
[13] F. Verluise, V. Laude, Z. Cheng, Ch. Spielmann, and P. Tournois, Opt. Lett. **27**, 707 (2000).
[14] I. Iaconis and I. Walmsley, Opt. Lett. **23**, 792 (1998).
[15] A. E. Siegman, *Lasers* (University Science Books, Mill Valley, CA, 1986).
[16] S. Kazamias, F. Weihe, D. Douillet, C. Valentin, T. Planchon, S. Sebban, G. Grillon, F. Aug, D. Hulin, and Ph. Balcou, Eur. Phys. J. D **21**, 353 (2002).
[17] K. C. Kulander, K. J. Schafer, and J. L. Krause, in *Super Intense Laser Atom Physics*, Vol. 316 of NATO Advanced Study Institute, Series B: Physics, edited by B. Piraux, A. L'Huillier, and R. Rzazewski (Plenum, New York, 1993).
[18] R. Taieb, V. Veniard, and A. Maquet, Phys. Rev. Lett. **87**, 053002 (2001).
[19] M. Lewenstein, P. Salieres, and A. L'Huillier, Phys. Rev. A **52**, 4747 (1995).
[20] Ph. Balcou, P. Salieres, A. L'Huillier, and M. Lewenstein, Phys. Rev. A **55**, 3204 (1997).
[21] M. V. Ammonosov, N. B. Delone, and V. P. Krainov, JETP Lett. **64**, 1991 (1986).